Faculty
of Science

Structural and chemical properties of boron and nitrogen dopants in graphene by means of STM/AFM in UHV at 5 K

Master Thesis

Author: Bc. Benjamin Mallada Faes

Supervisor: Ing. Pavel Jelínek, PhD.

Consultant: Bruno de la Torre Cerdeño, PhD.

Department of Physical Chemistry, Faculty of Science

Palacký University

2019

Declaration

I hereby declare that I completed my master's thesis independently under supervision of Ing. Pavel Jelínek, PhD. and all sources are included in the bibliography. **Bc. Benjamin Mallada Faes**

Olomouc .....

Key words: STM, AFM, KPFM, doped graphene, nitrogen doped graphene, boron doped graphene, graphene reactivity with CO.

Acknowledgments

I would like first to thank my supervisor Ing. Pavel Jelínek, PhD. for offering me the opportunity of working in his group and for supporting me in my Master studies. I would like also to thank Bruno de la Torre Cerdeño, PhD. for teaching me how to measure in an STM/AFM at 5 K and also for his help in measuring, processing and writing down the data that appears in this master thesis. Also, I would like to thank Martin Švec, PhD. for teaching me the basics of STM/AFM at room temperature. I am also very thankful to Mgr. Petr Lazar, Ph.D. for performing the DFT calculation of the dopants on graphene. To our new colleague, Hector Gonzalez Herero, Ph.D. thanks for the interesting conversations in the lab and also for the technical help.

Special thanks go to prof. RNDr. Michael Otyepka, Ph.D. for all his support during my master studies and to prof. RNDr. Radek Zbořil, Ph.D. for having the opportunity of working with the new STM/AFM machines in the RCPTM.

I am very grateful with Jesus Redondo for introducing me into the research world by suggesting me to take an Erasmus Internship a couple of years ago, and for his support at working and personal level. Additionally, he grew and doped the graphene used in this master thesis. To my colleagues Aurelio Gallardo and Shayan Edalatmanesh, it was nice to work with you, thanks for the AFM simulations and related calculations. I would like to thank also Taras Chutora for his always fruitful discussions about related and not related topics to STM/AFM and I wish him luck in his next professional steps. Last, I would like to thank Daniela for her personal and emotional support while studying and doing research, especially for her understanding!.

To my mother, that always supported any path I wanted to follow, I am beyond grateful.

BIBLIOGRAPHIC IDENTIFICATION

Author: Bc. Benjamin Mallada Faes
Title: Structural and chemical properties of boron and nitrogen dopants in graphene by means of STM/AFM in UHV at 5 K
Type of thesis: Master Thesis
Supervisor: Ing. Pavel Jelínek, PhD.
Department: Department of physical chemistry and Regional centre of advanced technologies and materials, Palackyé University, Olomouc
Year of presentation: 2019
Abstract: During the last decade, graphene has emerged as one of the most researched material with promising applications in photocatalysis, molecular sensing, nanoelectronics, and energy storage. Here we show the incorporation of substitutional dopants significantly affects the graphene chemical reactivity. B and N dopants locally reduce and increase respectively the interaction of graphene to individual CO molecules attached to the apex of metallic tip, used for performing scanning probe microscopy and atomic force microscopy. The interaction is driven by weak electrostatic forces between seated charges induced by dopants in graphene and the molecule. The doping is accompanied by a sharp redistribution of graphene electron density at the B-C and N-C bonds observed in high-resolution AFM images and subsequent variation of the work function. Our observations provide further insight into the non-covalent interactions of boron and nitrogen dopants in graphene with relevant molecules for potential applications in molecular sensing.
Key words: STM, AFM, KPFM, doped graphene, nitrogen doped graphene, boron doped graphene, graphene reactivity with CO.
Language: English
Number of pages: 59

Summary

During the last decade, graphene has emerged as one of the most researched material with promising applications in photocatalysis, molecular sensing, nanoelectronics, and energy storage. Graphene, a one atom thick layer of carbon atoms in a honeycomb structure, exhibits novel mechanical and electronic properties as zero band gap, ballistic charge carrier, fractional quantum Hall effect, etc. However, addressing specific technological applications required controlled modification of graphene properties at the atomic level.

Among others, the doping of graphene with heteroatoms has become one of the most successful routes for tuning its electronic and chemical properties. In particular, the incorporation of substitutional boron (B) and nitrogen (N) atoms in the graphene lattice, leads acceptor and donor centers of charge carriers respectively modifying its electronic properties. Beyond a shifting of the Fermi level, B and N dopant centers strongly affect charge and phonon transport and induce magnetism in graphene. However, up to the best of our knowledge, detailed insight into the impact of B and N dopants in graphene chemical properties is missing so far.

Here we show the incorporation of substitutional dopants significantly affects the graphene chemical reactivity. B and N dopants locally reduce and increase respectively the interaction of graphene to individual CO molecules

attached to the apex of metallic tip, used for performing scanning probe microscopy and atomic force microscopy. The interaction is driven by weak electrostatic forces between seated charges induced by dopants in graphene and the molecule. The doping is accompanied by a sharp redistribution of graphene electron density at the B-C and N-C bonds observed in high-resolution AFM images and subsequent variation of the work function. Constant-height maps of the local contact potential difference acquired with Kelvin Probe force Microscopy showed electrostatic charge associated with dopants centers. The experimental findings are fully supported by total energy DFT calculations and molecular mechanics simulations.

Our observations provide further insight into the non-covalent interactions of boron and nitrogen dopants in graphene with relevant molecules for potential applications in molecular sensing.

Contents

List of Figures

1 Introduction

Graphene had been extensively studied as a result of its attractive physical properties [1, 2], however nowadays the interest has been focused on materials based on the chemical functionalization of graphene [3] due to the low reactivity of graphene to molecular adsorbents. Controlled modification of graphene physicochemical properties opens a new route for the development of customized materials towards tangible applications such as energy conversion/storage devices [4], molecular sensors [5], biomedicine [6] and photovoltaic [7] among others.

1.1 Graphene

Graphene is a two-dimensional material composed of a single layer of carbon atoms arranged in a honeycomb lattice. Its isolation and first characterization was achieved in the University of Manchester in 2004 and awarded Geim and Novoselov [1, 2, 8] a Nobel Prize in 2010. Additionally to its properties, graphene is also considered the first isolated 2D material [9] and has opened new routes for developing nanomaterials. In graphene, the honeycomb lattice can be described in terms of a primitive lattice containing two atoms, A and B, (see Figure.1) where each carbon atom of the lattice has three sp^2 hybridized orbitals and one p_z orbital. The sp^2 orbitals are responsible for

the bonding between carbon atoms by covalent σ-bonds (Fig.2) and confers its structural strength to graphene, while the p_z orbitals, perpendicular to the graphene lattice, forms π-bonds, building up the π-band and $\pi*$-bands, responsible of the electronic properties of graphene, such the zero-band-gap of graphene and its semimetallic character [10].

These two kinds of bonding are the main responsible of the structural and electronic properties of graphene, such the high mobility of charge carriers [11], large Young modulus [12], excellent thermal conductivity [13] and also the possibility of being functionalized with functional groups and heteroatoms [14].

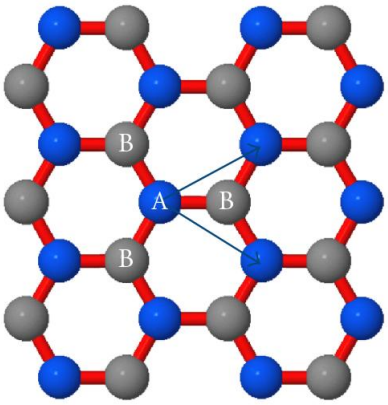

Figure 1: The primitive cell of graphene lattice containing atoms A and B. Adapted from [10].

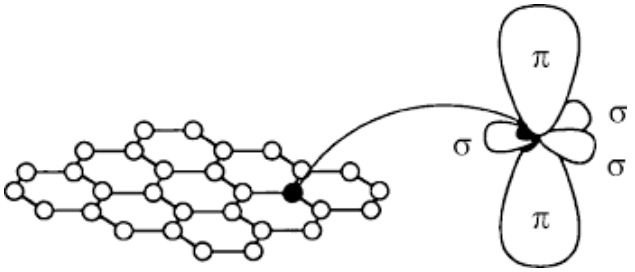

Figure 2: The sp^2 hybridization of graphene. Adapted from [15].

1.2 Doped graphene

Therefore, tuning the chemistry of graphene could promote this material for applicable new properties on demand. Apart from its intrinsic capabilities, modified graphene exhibits interesting new properties such as superconductivity, ferromagnetism, non-linear optical response or enhanced chemical reactivity [3].

Tailoring electronic and chemical properties of graphene could be attained by different routes involving subtle modification of carbon sp^2 lattice by adding functional groups via covalent and non-covalent interactions or implantation of heteroatoms (i.e. boron, nitrogen, sulfur, phosphorus...) in the graphene basal plane.

Of the different mechanisms for controlling the chemical properties of graphene, the so-called doping is a primary chemical modification which involves substitutional heteroatoms (dopants) implanted into the graphene lattice or intercalated into the graphene-substrate interface. Many types of

dopants have been successfully implanted and/or intercalated providing a wide range of new properties to graphene. Among the different atoms and configurations in graphene, substitutional boron and nitrogen dopants have attracted most of the interest due to their similar atomic radii to carbon. Nitrogen has been widely employed for inducing n-type character to graphene conductivity [16] and, therefore, is a cornerstone for future microelectronic applications. Additionally, it has been observed that substitutional nitrogen dopants can enhance the reactivity of graphene to certain electrochemical processes such as oxygen reduction reaction [17]. The vast knowledge obtained in the synthesis of this material leads to several novel applications in diverse fields.

On the other hand, boron doping represents a complete distinct scenario from an electronic point of view [18]. Its lower electronegativity induces p-type conductivity to graphene. Despite the fact boron-doped graphene (B-G) may stimulate new chemical and electrochemical activity to the graphene layer, the efforts has produced less progress than on nitrogen-doped graphene (N-G) and only very recently has accomplished the same degree of ripeness and development in terms of synthesis, physicochemical characterization [19, 20], and technological applications.

Due to its 2D character, graphene and its functionalized derivatives are currently often used as components in graphene-molecule systems [21]. In

general, the graphene-molecule boundary phenomena are well observed due to a large sensitivity of response of intrinsic electrical and electrochemical properties of graphene to variations in its local chemical environment, and for this reason, graphene has been found attractive for sensing a vast variety of molecules and gas vapors [22, 23, 24].

It is accepted that adsorption of gas molecules onto the graphene surface promotes alteration in local carrier concentration induced by donor/acceptor character of adsorbates. Graphene-based sensors can detect individual events of adsorption/desorption of molecules from the surface by step-like changes in graphene resistivity [25]. Importantly, the sensing capability can be improved by introducing defects and dopant sites in graphene with higher affinity to selected molecules [26]. On top of this, graphene is a suitable substrate for imaging molecular self-assembly and study intermolecular interactions [27, 28, 12, 29, 30, 31]. The establishment of weak, mainly van der Waals, interactions between molecules and graphene surface do not alter the self-assembly mechanisms while retaining the essential electronic features of the molecular layer [32]. Notably, the introduction of functional groups or dopant sites may alter the interacting landscape of pristine graphene inducing both geometric and electronic structure modifications of the adsorbed molecules. Thus, doped graphene may act as a non-covalent tuner of the electronic properties of adsorbed molecules.

We need high-resolution techniques of surface science for characterizing these properties. In this thesis, we will conduct a research on the chemical reactivity of substitutional boron and nitrogen in graphene by means of STM/AFM for providing deeper insight on the chemical properties of the dopants at the atomic level. Herein, Scanning tunneling microscopy (STM) and Atomic force microscopy (AFM) become powerful tools for characterizing the chemical, electronic, structural and mechanical properties of doped graphene at the atomic scale.

2 Methods

In this section, we will present a basic introduction to the methods for growing and doping of graphene on SiC(0001) and the techniques for the characterization this grown codoped graphene.

2.1 Graphene growing on SiC(0001)

To address the purpose of the present master thesis, we study graphene growth on a 6H-SiC(0001) wafer by a stepwise graphitization in UHV conditions. A first thermal annealing at T >1020 K, in a Si enriched atmosphere, leads to the sublimation of Si atoms from the surface promoting the growth of a first carbon layer (see Figure.3), called *Buffer layer* (BL). The BL is weakly bounded to the SiC(0001) surface and reconstructs in a quasi-periodic $6\sqrt{3} \times 6\sqrt{3} - R30^{\circ}$ honeycomb. This layer acts as the precursor of the following step. Posterior annealing up to T = 1520 K give rise the growth of single-layer graphene (SLG). The mechanism of growing of SLG on SiC (0001) is displayed in Figure.4.

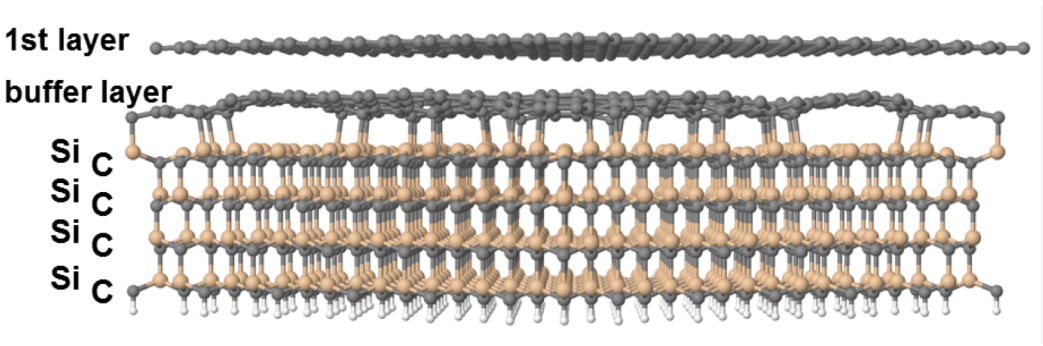

Figure 3: Relaxed model of a single layer graphene (1 st layer), buffer layer (BL) and 6H- SiC(0001) system. Adapted from [33].

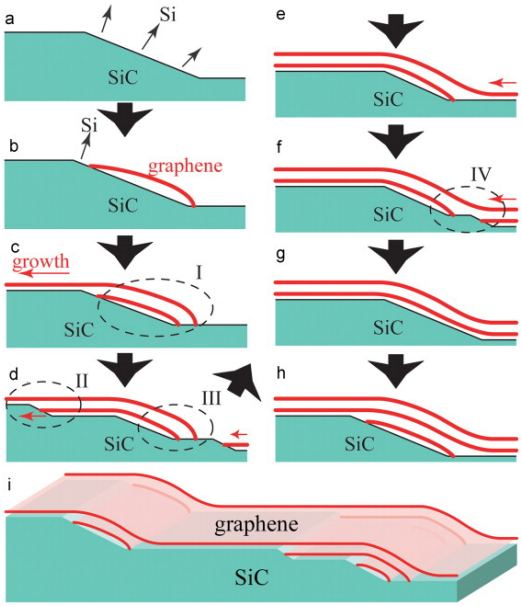

Figure 4: Growing model of single layer graphene on SiC(0001). Adapted from [34].

2.2 Boron and nitrogen doped Graphene on SiC(0001)

In this section, we introduce the two steps process of boron and nitrogen doping of G/SiC(0001). In the first step, graphene is doped with B by evaporation of metallic boron. In a second step, the implantation of N dopants

is done by means of nitrogen ion sputtering. Each of these steps is described in the following sections.

2.2.1 Boron doping

The doping with boron of graphene was carried as described in Sforzini and coworkers [20]. After growing G/SiC(0001) in an external secondary uhv chamber, the boron doping is achieved by sublimating metallic boron from a commercial evaporator on already grown graphene at room temperature and finished with final annealing at 1420 K for 20 minutes. This procedure incorporates substitutional boron dopants in graphitic positions of the graphene lattice up to a maximum concentration of 0.1 %.

2.2.2 Nitrogen doping

The doping with nitrogen starts with the transfer of the B-doped sample from the secondary UHV chamber where is prepared, to the preparation chamber of the microscope. This transfer between chambers is done at atmospheric pressure due to the great stability of graphene grown on SiC(0001). After introducing the sample to UHV conditions (see Fig.5), the sample is annealed up to 800 K in order to remove impurities. The N implantation is done by sputtering of the graphene sample with N^+ ions accelerated at 120 eV. In a second step, subsequent annealing up to T = 1070 K (see Fig.5) allows to

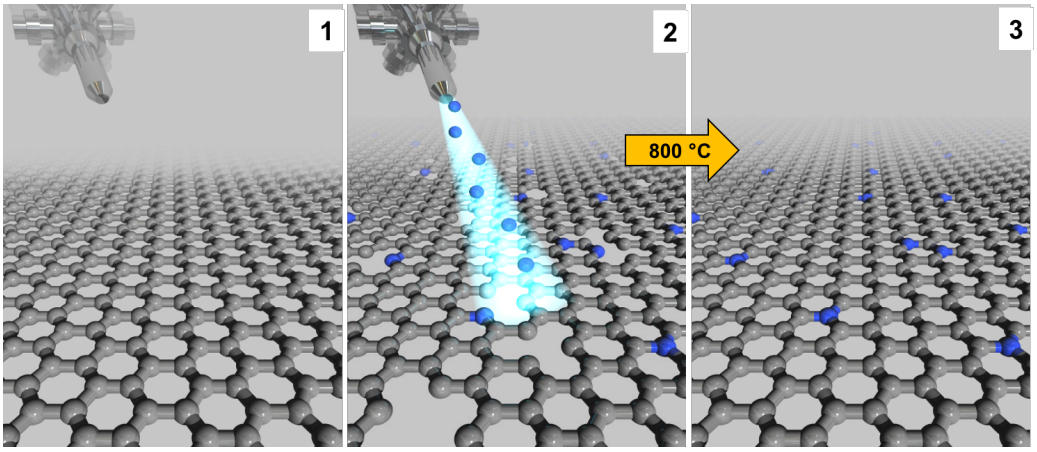

Figure 5: Nitrogen doping scheme. Adapted from [20].

implant the N into the graphene lattice.

2.3 Scanning Tunneling Microscopy

The Scanning Tunneling Microscopy is a technique invented and developed at IBM Zurich Research Laboratory in 1981 by Binnig and Rohrer [35], awarded in 1986 with a Nobel Prize, that enables the imaging in real space and study of surfaces with atomic resolution. The principle of this technique is based on the quantum tunneling effect through a potential barrier. A sharp metallic tip is approached to a metallic or semiconducting surface, with picometer precision. By applying a potential difference (i.e. Bias voltage), a current rises due to the non-zero probability of electrons tunneling through the vacuum gap. This current depends exponentially with the distance between tip and sample (i.e. decreasing the distance 1 Å increases the current in

one order of magnitude) and it is the principle that gives STM its spatial resolution. In this thesis, we will only consider one mode of measurement, the constant current mode. In this mode, the tip-sample distance is controlled by a feedback loop keeping constant a pre-defined value of current (e.g current setpoint) and the measured signal is the vertical movement of the tip. Displacing the tip across the sample produces a topographic map of the sample.

2.4 Atomic Force Microscopy

The Atomic Force Microscope (AFM) is a technique developed in the 80s by Binnig, Quate, and Gerber [36] in IBM Zurich Research Laboratory, where the imaging mechanism is the forces acting between the scanning probe and the surface sample. A tip is mounted on a cantilever free edge. When approaching to the surface, the force sensed by the tip is expressed as mechanical deflections on the cantilever. These deformations can be monitored by means of different detectors and converted to an electrical signal proportional to the tip-sample interaction. In this thesis, we use qPlus sensors [37] (Fig.6), which uses the piezoelectric effect of a quartz tuning fork for monitoring the dynamics of the cantilever. In addition, the use of metallic tips allows acquiring simultaneously STM/AFM.

We used frequency modulation (FM) mode which permits to resolve structures with atomic resolution in UHV. In FM the cantilever oscillates at a constant amplitude (A) in resonance. The proximity of the sample produces shifts in the resonance frequency Δf due to the interacting forces, which normally can be described by a Lennard-Jones potential. Maintaining the system in resonance leads to the following solution for the cantilever dynamics in the case of small amplitudes (A $>$ 1 nm):

$$\Delta f = \frac{-f_0}{2k}\frac{\partial F}{\partial z} \tag{1}$$

Where Δf is the frequency shift, f_0 is the resonance frequency, k the elastic constant of the tip, F the force and z the distance between tip and sample. In the present thesis we use oscillation amplitudes of $\approx$ 50 pm and qPlus sensors with k$\approx$ 1800 Nm and a resonance frequency f_0 $\approx$30.000 Hz that allows us to measure forces with pN resolution. However, for arbitrary amplitudes, there are no analytic solutions for deconvoluting the force from the Δf and approximations must be considered as the Matrix method [38] or the Sader-Jarvis method [39].

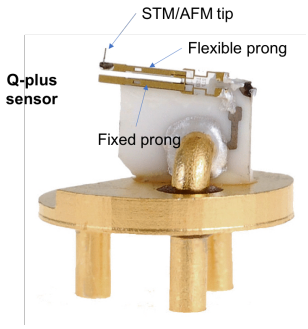

Figure 6: QPlus sensor. Adapted from [40].

2.5 Kelvin Probe Force Microscopy

The Kelvin Probe Force Microscopy (KPFM) is a scanning probe method derived from dynamic AFM that enables measuring the local work function of a sample. The principle of this technique is explained in the energy diagrams of Figure.7 in the left panel. A conducting tip and a sample, with different work functions W_{tip} and W_{sample} share the same vacuum level. If the tip and the sample are electrically connected, an electric current will flow from the element with the higher work function to the element with the lower one until their Fermi energies are aligned (central panel)). The difference of work functions ΔW leads therefore to a voltage drop $V^* = \Delta W/e$. At this point, an electrostatic force appears between tip and sample due to the built electric field across the vacuum barrier between them. This electrostatic force is experimentally measured as a change in Δf (right panel). By applying an external electric field, the electrostatic force evolves following a parabolic

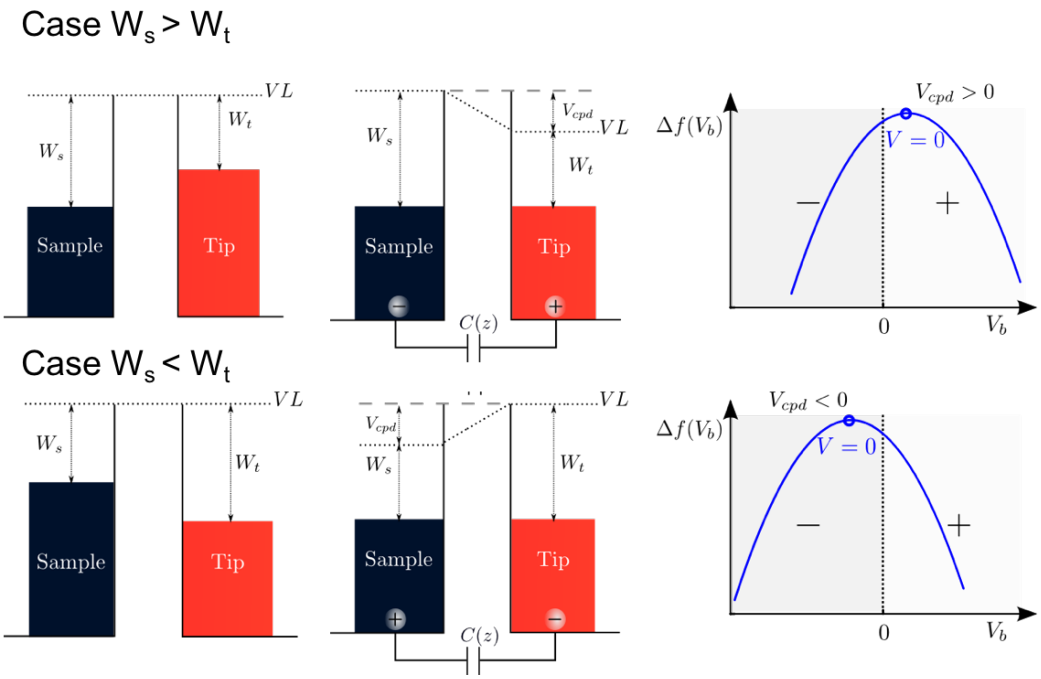

Figure 7: Schematic picture of the Kelvin Probe Force technique. In the top row, the case of a tip with a lower work function than the sample work function. In the bottom row, the case of a tip with a lower work function than the sample work function. The parabolas in both cases show the evolution of the frequency shift Δf for a variable applied voltage and their relative shifts.

path. The value of the voltage that minimizes the electrostatic field between tip and sample is called *local contact potential difference* (LCPD) and is equal to the difference of work functions ΔW between tip and sample. Additionally, it has been shown by Gross and coworkers [41] that it is possible to relate the shifts of the KPFM parabolas to the sign of localized charges. Therefore, the value of LCPD provides information on the work functions and charge distribution on a surface.

3 Results and discussion

The STM/AFM characterization of the doped graphene was performed in UHV at 5 K subsequent to the sample doping in a UHV preparation chamber with an STM-AFM tip apex functionalized with a single CO molecule. In STM topography (Fig.8-a), the periodic honeycomb structure of graphene is revealed (highlighted with color lines), along with the characteristic moire pattern of monolayer graphene induced by the $6\sqrt{3} \times 6\sqrt{3} - R30^{\circ}$ reconstruction of the underneath buffer layer [42, 43, 33].

The corrugation of graphene in STM topography (Fig.9), is measured to be in good concordance with previously reported results at room temperature [19], with an average value of 25 pm. In addition to the graphene lattice, boron and nitrogen graphitic dopants are randomly distributed as bright triangular features in good agreement with previous results [19, 44, 18, 43, 20]. The assignation of graphitic character to the dopants might be done by visual comparison with a honeycomb lattice extending from the unperturbed graphene to the feature sites.

Notably, the STM contrast of boron and nitrogen dopants features exhibits remarkable differences regarding the spatial extension over the graphene lattice. As evidenced in Figure.8-b and Figure.8-c, around the dopant sites arises a three-fold scattering with an spatial extension of up

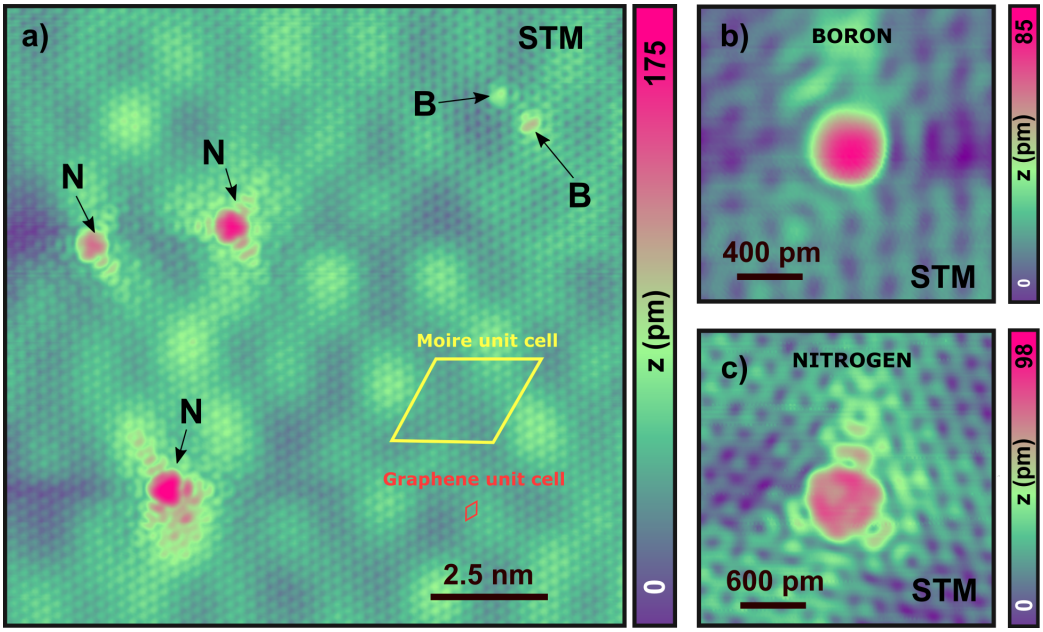

Figure 8: (a) STM high-resolution image of boron and nitrogen doped region. Both graphene lattice and moire superstructure are resolved and highlighted by color lines respectively. The image was acquired at constant current with a functionalized CO-tip (V_{Bias} = 300 mV, I_{set} = 100 pA). (b,c) STM detail of boron and nitrogen dopants respectively. A stronger scattering effect is observed for the N-dopant by comparison with the B-dopant.

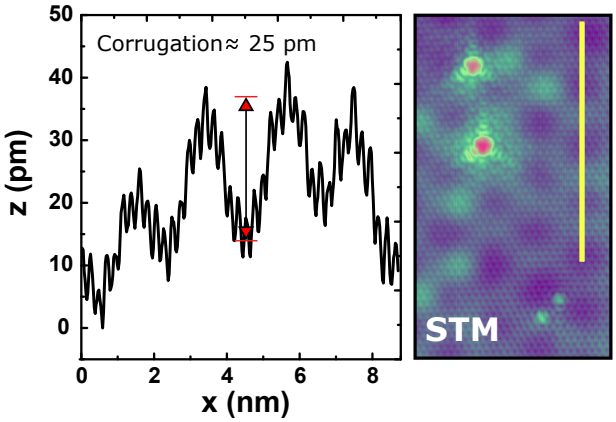

Figure 9: Topographic profile of pristine graphene (left panel). The profile was acquired along the yellow line displayed in the STM image (right panel), with acquisition parameters (V_{Bias} = 300 mV, I_{set} = 100 pA).

to 1 nm in the case of N and barely one unit cell in the case of B. In both cases, the three-folded symmetry scattering arises from the elastic scattering of π-band electrons with the dopants in graphene acting as defect centers. The difference in extension and intensity of the scattering are attributed to elemental differences between the dopants [42, 45, 46]. This may indicate a stronger influence of nitrogen to the quasi-free electron mobility in graphene in SiC(0001) in a different manner than observed in doped graphene on Cu substrates [44, 18]. In the later, the stronger interaction with the metallic substrate may plan a non-negligible role in the electronic properties of doped graphene.

STM images provide information via the local electronic density of states (LDOS), the features and contrast observed in STM may change with different applied bias voltage [47]. In order to study the influence of the applied voltage in the identification of objects in graphene, we acquired a series of STM images of the same doped region for different applied bias voltage. Figure.10 shows the filled and empty states of the same doped graphene region. For a bias of $\pm$ 0.1 V, the contrast of the BL in our STM images is reduced. For very low bias, only graphene and pure substitutional defects are resolved. Note that Bias = 0 V represents the energy position of the Fermi level.

Thus far, we have characterized co-doped graphene by means of STM imaging and also presented the limitations of the technique for a true local

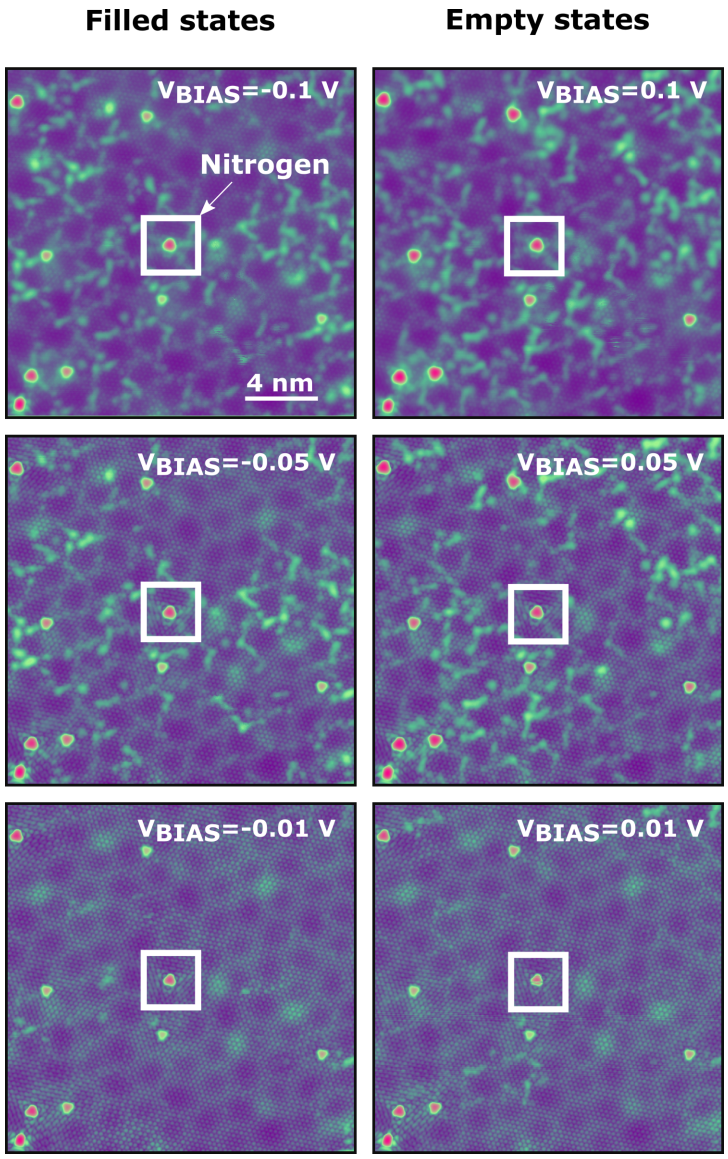

Figure 10: STM imaging of filled and empty states of N and B codoped graphene on SiC(0001). The white square encloses a nitrogen dopant for reference. All the images were acquired with $I_{set} = 20$ pA.

structural elucidation of dopants. Therefore, a comparison with other high-resolution surface techniques as TEM or non-contact atomic force microscopy (nc-AFM) is desirable. Since we are interested in studying the system without introducing other potential defects on graphene as occurs in HR-TEM imaging [48], nc-AFM appears as a more suitable technique. In addition, it allows the interaction between the tip and the dopants and therefore the study of the chemical reactivity of the dopants. In particular, the use of an inert functionalized tip in nc-AFM (e.g. CO-tip) allows non-invasive high-resolution imaging [49] of organic molecules, study of interactions between tip and surface atoms [50], to identify chemical structures [51, 52], the observation of intramolecular bonding for close tip-sample distances [51, 53], molecular spin state discrimination [54] and molecular bond order [55].

Figure.11-a shows an STM image acquired with a CO-tip of doped graphene containing three nitrogen and one boron dopant. As observed in STM images, boron and nitrogen dopants are featured with distinct contrast. Boron and nitrogen dopants are imaged brighter and darker respectively than the surrounding carbon atoms. This observation is in good agreement with recently reported co-doped boron and nitrogen graphene nanoribbons on Au (111), where the opposite contrast in both dopants is attributed to elemental differences [56].

The nc-AFM is sensitive to tip-sample interaction forces. These arise

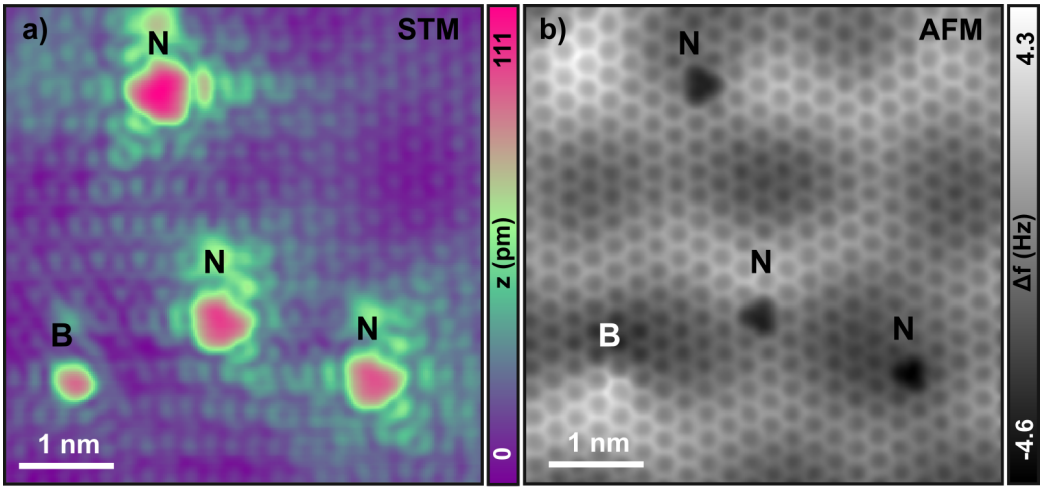

Figure 11: (a) STM topography image of a boron and nitrogen co-doped graphene area (V_{Bias} = 200mV, I_{set} = 50 pA). (b) High resolution constant height nc-AFM image of the same area displayed in (a) with one boron and three nitrogen. The boron dopant appears as a bright dot (bottom left corner) while nitrogen appears as dark triangles.

from the interplay between Pauli repulsion, electrostatics and van der Waals interactions sensed at a fixed tip-sample distance. Thus, in order to get further insight into the origin of the observed contrast, Figure.12 shows a series of detailed experimental nc-AFM images acquired individually for each dopant at different tip heights (z) with exactly the same tip. We intentionally selected dopants located in similar positions respect to the graphene moire superlattice.

From far distances (z > 120 pm), a brighter (less negative frequency shift Δf) contrast is resolved for boron site (Fig.12-a 'Experimental'), while for nitrogen a darker (more negative frequency shift) contrast is observed (Fig.12-b 'Experimental'). Upon tip approach (90 pm > z > 75 pm), graphene rings

are clearly resolved in the images, and in addition, the three C-B bonds are comparatively brighter than the surrounding C-C bonds. In the other hand, for the nitrogen dopant, no significant C-N bond is observed and a dark triangle around the nitrogen atom site is displayed. Decreasing further the tip-sample distances (z $<$ 60 pm), on the boron site the three C-B bonds show a similar contrast to the C-C bonds whereas, on nitrogen site, the N-C bonds start to be resolved. This contrast is observed with several CO-tips regardless of the N and B exact position in the moire.

The observed contrast dependence is corroborated by theoretical simulation. Our collaborators performed AFM imaging simulations of boron (Fig.12-a 'Simulated') and nitrogen(Fig.12-b 'Simulated') dopants based on a numerical model (Probe Particle) which takes into account the charge and the relaxation of the CO-probe [57] with the doped graphene structure and the electron densities calculated by total energy DFT. The simulations are in excellent agreement with the experimental images, capturing the brighter and darker contrast of the C-B and C-N bonds respectively. Not only that, but the model also reproduces the contrast dependence with the CO-tip separation of the experiment, showing negligible vertical relaxations of the graphene layer at the nitrogen and boron atom sites when incorporated in graphitic configuration, therefore discarding a topographic origin for the contrast difference.

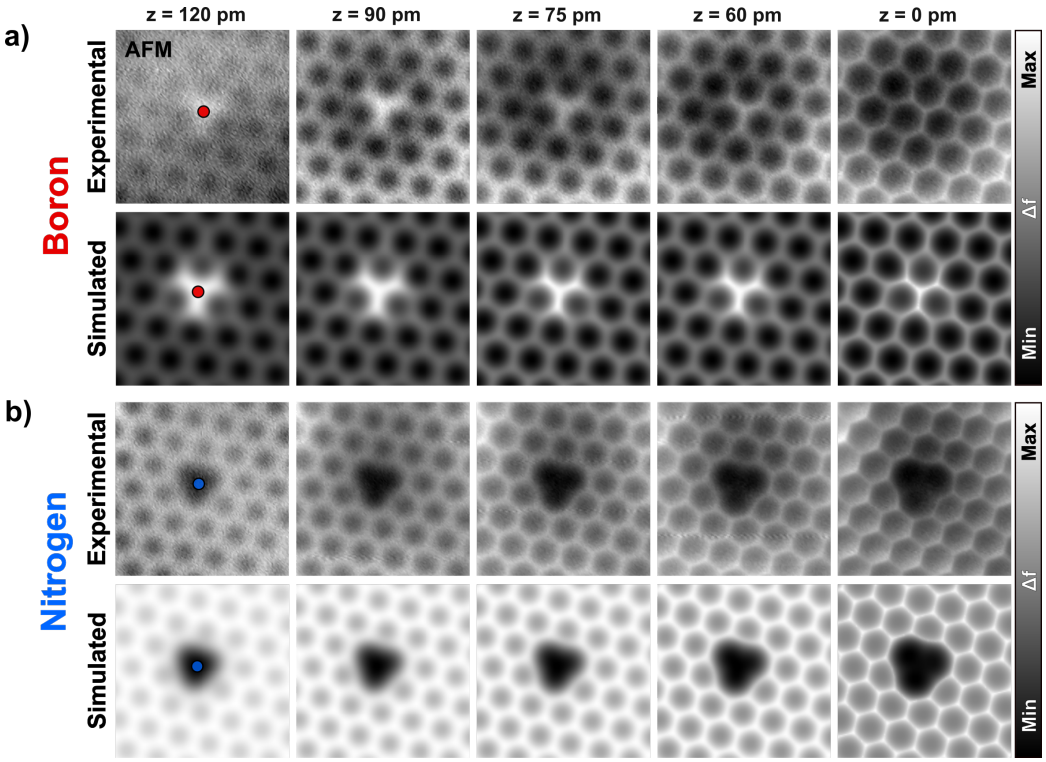

Figure 12: Experimental and simulated constant height AFM images of boron dopant (a) and nitrogen dopant (b) as a function of the tip-sample separation. Tip-sample distance decreases from left to right up to 120 pm. Blue and red dots mark the exact position of the boron and atom atoms respectively. The origin z = 0 corresponds with a tip approach of 150 pm from the STM setpoint (V_{Bias} = -500 mV, I_{set} = 50 pA).

At small tip-sample distances, AFM with CO-tips maps the spatial variations of the potential landscape which can be linked to electron densities [58]. Thus, changes in the contrast can be related to sharp variations of the electron densities. Indeed, it is expected that the incorporation of donor/acceptor centers must be accompanied by a charge transfer. The lead/accommodation of extra charge to/from graphene induce a variation in electron densities which are located around the dopant sites.

Therefore, the chemical interaction between dopants and the CO tip might be further explored by AFM site-specific force spectroscopy. In order to explore the chemical reactivity of the dopants, the frequency shift Δf is recorded as a function of the distance z between the CO molecule and the specific site with picometer resolution. We intentionally selected dopants in equivalent graphene sites to void any topographical effect and performed force spectroscopies as seen in Figure.13 over boron (red), nitrogen (blue) and carbon (yellow) atoms.

For large distances (z $>$ 250 pm), no significant differences are observed in spectroscopies above carbon, nitrogen and boron atoms. For closer separation, (z $<$ 150 pm), a small difference between spectroscopies is resolved, measured as a less/more negative frequency shift Δf (less/more attractive interaction) for boron and nitrogen dopants. This is in correspondence with the contrast developed in the AFM images (Fig.12). Near the minima (z $\approx$

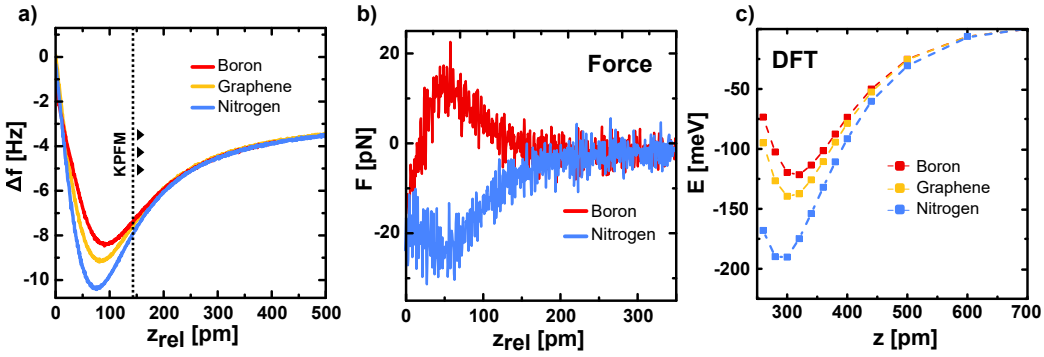

Figure 13: (a) Experimental Δf(z) spectroscopies (solid line), acquired CO-tip above the B (red) and N (blue) dopants in graphene (yellow). (b) Deconvoluted force between the CO-tip and the boron (red) and the nitrogen (blue) dopants. The signal of graphene was subtracted from the spectroscopies. (c) DFT calculated interaction energies between a CO-tip and the dopants in graphene.

80 pm), clear differences are seen for both dopants, with nitrogen exhibiting the largest attractive interaction followed in order by carbon and boron atoms.

Since force spectroscopies do not provide a direct quantification of the forces involved in the interaction, indirect methods for calculating the experimental values must be considered. The reason for this is that in the FM-AFM mode, the measured signal is proportional to the gradient of the force and not directly to the force [38] (see Section. 2.4). As a result of this, calculating quantitatively the force (Fig.13-b) requires a deconvoluting process as has been described by Giessibl [38].

In our spectroscopies, we noticed that commonly used methods for long-range subtraction may introduce a large dispersion of the calculated values.

Instead, long-range site independent van der Waals and electrostatic forces were not removed by commonly used methods based on fitting plots which may introduce a large dispersion in the calculated force. Instead of, the variation of the short-range chemical interaction was quantified by subtracting the force spectroscopy Δf(z) measured above of a carbon atom from the Δf(z) spectroscopy measured on top of each dopant. This procedure removes non-specific site interactions, giving us a quantification of the chemical reactivity variation induce by dopants in graphene to a CO molecule. We observe an increased attractive force on top of the nitrogen dopant of around 25 pN than on a carbon atom. On the other hand, the interaction of CO and boron atom is circa 15 pN less attractive. Despite this rather small force differences, AFM is sensitive enough to image the exact configuration of the dopants in graphene and also to provide information about the strength of the interaction.

These observations are in agreement with our collaborator calculations. We fully support the experimental findings by DFT + vdW calculations performed using the projector-augmented wave method in the Vienna Ab initio Simulation Package (VASP) [59, 60]. The surface of graphene was modeled using a supercell of 5×5 elementary cells (50 carbon atoms). The tip was modeled with a CO molecule attached to the apex gold atom of a triangular pyramid Au cluster (10 Au atoms) having Au(111) faces. The

topmost layer of an Au cluster and two atoms of graphene were fixed, while the rest of the system (CO molecule and adjacent Au atoms, graphene atoms beneath the tip) were allowed to vertically relax. We used optimized van der Waals functional optB86b-vdW [61] in all calculations, which provided a balanced description of van der Waals and covalent bonding in previous studies [62].

In Figure.13-c is plotted the vertical energy component for the calculated tip-sample interaction energy, in an excellent qualitatively agreement with the experimental findings (z indicates the distance between the layer and the Oxygen atom in the CO-tip). The plot shows larger interaction energy for the CO-tip on the nitrogen atom (ca. 190 meV) followed by on the carbon atom (ca. 140 meV) and the boron atom (ca. 120 meV). Although the exact value of the calculated interaction energy is quantitatively sensitive to the description of the van der Waals potential, the order N > C > B remains the same for the inspected functional.

Thus far we have been considering the total interaction between the CO-tip and the boron and nitrogen dopants. This is an interplay of long and short-range interactions. In the long-range, van der Waals, electrostatic and magnetic interactions are the dominants whilst for short range is mainly, electrostatic, chemical forces and Pauli repulsion. Of these, the long-range interactions are non-site specific and have no direct impact on the AFM imag-

ing of the dopants as can be observed in the loss of contrast in AFM for long distances (Fig.12) and in force spectroscopies (Fig.13). In the other hand, the chemically inert CO-tip discards a chemical origin for the imaging in the short range, while the Pauli repulsion is expected to play a dominant role only at very close distances (z <50 pm). Therefore, the contrast observed in AFM images (0 < z <120 pm) is attributed to electrostatic forces originated by the charge distribution induced by the dopants.

This observation is corroborated by our Kelvin Probe Force Microscopy (KPFM) measurements with CO-tip over each dopant. This technique allows studying the differences in work function between the tip and the sample by recording changes of the frequency shift Δf with a variable bias voltage. In addition, KPFM experiments enable studying the charge of individual atoms on isolating surfaces [41] and also the characterization of charge distribution on molecules [63]. The frequency shift dependence on the applied bias Δf (V) follows approximately a square-law, $\Delta f(V) = a \cdot (V_{Bias} - LCPD)^2 + c$, where a is a parameter depending of the shape of the tip, V_{Bias} is the applied bias voltage, LCPD is the local contact potential difference that must be applied to minimize $\Delta f(V)$ and c is an offset accounting differences in the distance between tip and sample.

The performed KPFM parabolas for each dopant are displayed in Figure.14. The parabolas (Fig.14-b) for boron (red), carbon (yellow) and ni-

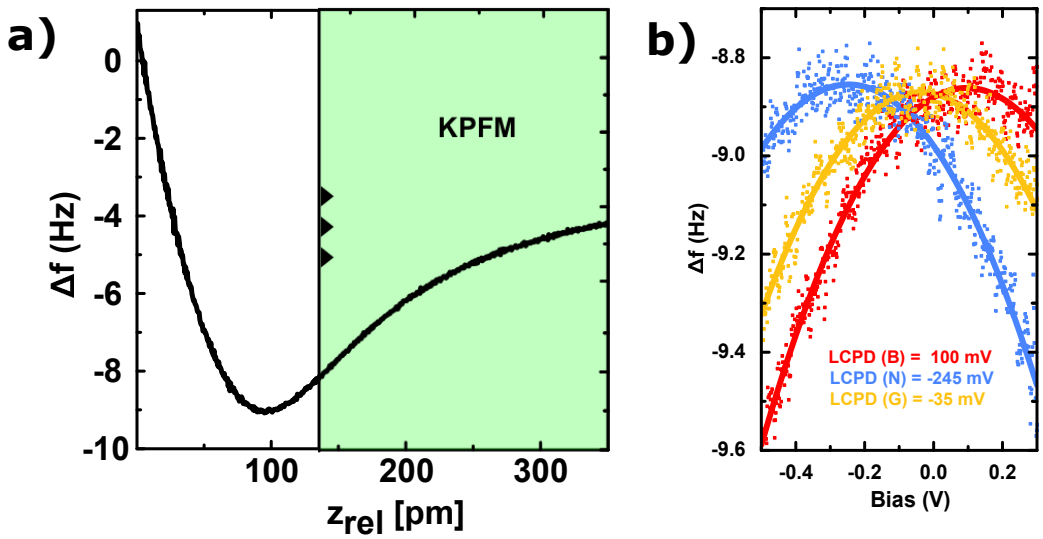

Figure 14: (a) Force spectroscopy of graphene showing the starting point for the acquisition of KPFM parabolas. Here, the origin corresponds to a CO-dopant distance of 140 pm from the closest AFM image. (b) KPFM parabolas measured over the boron (red), carbon (yellow) and nitrogen (blue) at the same tip-sample distance. Errors in LCPD fittings are about 1.5 mV.

trogen (blue) reveal a positive shift for the boron parabola and a negative shift for the nitrogen parabola respect to the graphene signal. By fitting the parabolas with a square law, we observe a substantial variation of the LCPD values for boron/nitrogen, shifting to higher/lower values (100 mV and -245 mV respectively) reflecting the increase/decrease of the work function on the dopants [41]. This observation can be rationalized by considering variations of the surface dipole induced by localized charges around the dopant sites. Quantitatively, LCPD values crucially depend on the mesoscopic tip termination due to long-range electrostatic forces [64], but we always observe a larger/smaller LCPD value for boron/nitrogen when compared to that on

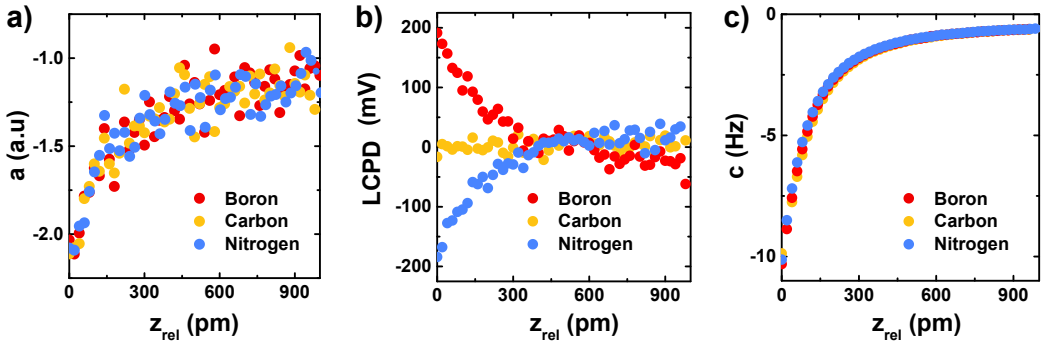

Figure 15: KPFM fitting parameters as a function of distance z. (a) The a(z) parameter. (b) Local contact potential difference (LCPD) as a function of z. (c) The c(z) parameter. The origin (z = 0) corresponds with the starting acquisition line displayed in Figure.14.

graphene.

In Figure.14-a, a force spectroscopy on graphene is displayed showing the closest distance (z = 140 pm) for which the KPFM was performed. For closer tip distances (Δz < 140 pm), the lateral movement of the CO on the tip due to the repulsive forces may induce distortions in the parabolic shape of the Δf(V) [63].

In Figure.15 are depicted the fitted parameters for each KPFM parabolas over each dopant as a function of the CO-sample distance. In Figure.15-a are displayed the values of the parameter a(z) for each dopant, related to the shape and electronic properties of the tip, with no perceivable differences over the different dopants. The LCPD(z) values in Figure.15-b clearly shows the differences of values for short distances over boron (red) and nitrogen (blue) and the loss of resolution in distances greater than (z > 300 pm). The

graphene signal (yellow) was subtracted in both plots in order to visualize the relative changes of each dopant compared to graphene. Last, the parameter c(z), related to the offset of heights, is plotted to show no remarkable differences between dopants.

To reach a deeper understanding of the spatial charges redistribution, we performed a 2D-LCPD mapping over a region containing one boron and one nitrogen dopant. We performed a full set of Δf(V) spectra at different tip-sample separations along a graphene line containing a boron and a nitrogen dopant (Fig.16- inset). In a posterior analysis, we proceed to the extraction of the LCPD values for each parabola in every point of the XZ plane with a Python script.

With the purpose of enhancing the visualization of the local variations of work function, we subtracted the background LCPD measured on pristine graphene areas. The resulting LCPD map is shown in Figure.16.

At the closest tip-sample distances (Δz = 140 pm), boron and the nitrogen atoms are featured with almost equal but opposite sign LCPD, with the boron acting as a negative charge and the nitrogen as a positive charge, following the relationship between LCPD shift and the sign of the charge described by Gross *et al* [41].

The net charge on the boron/nitrogen dopant is originated from the acceptance/donation of electrons to the linear graphene pi-band [20] and its

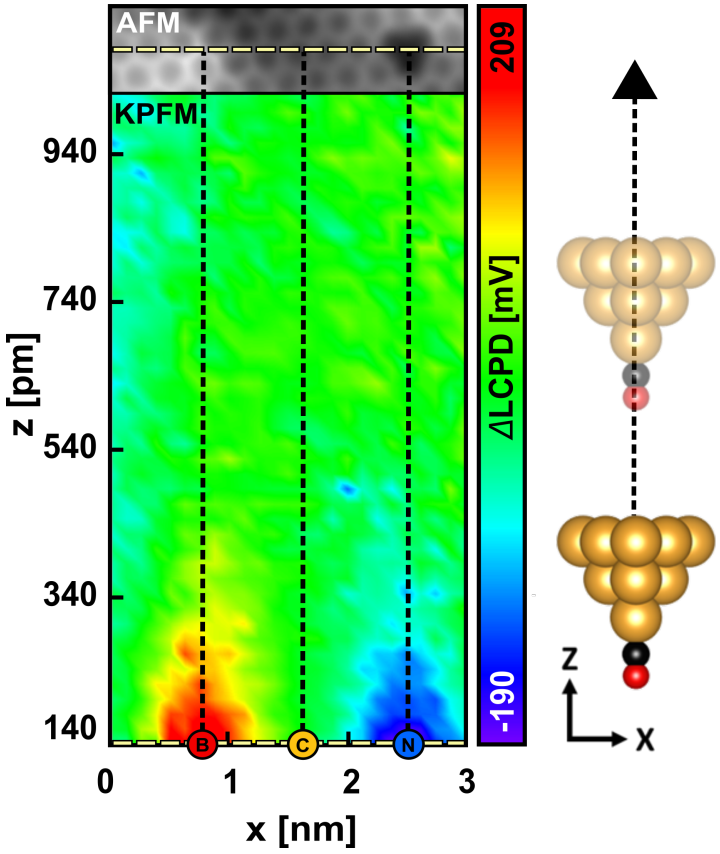

Figure 16: LCPD 2D-map at different tip-sample separations z along a line x which contains a boron and a nitrogen atoms (yellow dashed in the inset). Each pixel corresponds with the fitted LCPD value of the KPFM parabola acquired in every (x, z) position. The AFM inset shows the line in the x along along the data was acquired.

subsequent impact on the surface dipole. This points to a similar magnitude of the dopant-induced charge carriers transfer, in good agreement with previous experimental results [44, 18]. In addition, the LCPD map shows the spatial confinement of the charge on which extends laterally about 0.4 nm around the dopant site. As the tip-sample distance increases, the LCPD value on dopants decreases continuously up to separations higher $\Delta z = 290$ pm where the average graphene work function is predominant. Thus, the LCPD map highlights the lateral and vertical confinement of a net charge in a small volume centered on each dopant atom.

Interestingly the in-plane component of the induced electrostatic force field may be useful for tuning the scattering with charge carriers in graphene [65, 66, 67] while the out of plane component dominates the chemical reactivity providing selective sites for graphene functionalization with organic molecules [68, 69, 70, 54, 71].

4 Conclusions

In this master thesis, we have conducted a detailed investigation on the chemical properties of substitutional nitrogen and boron dopants in graphene on SiC(0001) by means of both experimental STM/AFM/KPFM measurements at 5 K with a functionalized CO-tip and theoretical calculations. The comparison between STM and AFM images acquired in the same sample region allows us to assign unambiguously imaging features to pure graphitic boron and nitrogen dopants. The former shows a bright contrast in AFM and small electronic structure in STM images. On the other hand, the nitrogen dopant leads to dark contrast in AFM and larger electronic structure in STM images. Interestingly, the sharp AFM contrast of C-B and C-N bonds show a clear tip-sample distance dependence which is attributed to the interplay of short-range forces and the renormalization of electron density around the dopant site in perfect agreement with theoretical simulations.

Next, we investigate the chemical interaction between a single CO molecule attached to the probing tip and N and B dopants comparing to that on graphene. While N dopant increases the graphene interaction to CO molecule of about 25 pN, B dopant reduces it in a value of about 15 pN. This indicates that both dopants investigated in this master thesis modify a little the graphene chemical reactivity. Indeed, our DFT calculations not

only confirms the increased/reduced reaction of nitrogen/boron dopants but also predicts very low to CO molecules which is within the range of 100-190 meV. In addition, both experimental force spectra and calculations point out to weak electrostatic forces responsible for site-dependent interaction of CO to the doped graphene.

At last, we further investigate electrostatic forces in doped graphene by means of KPFM measurements. LCPD parabolas obtained above nitrogen and boron dopants lead a distinct difference in local work function. Nitrogen/boron dopant reduces/increases the work function of graphene giving rise to positive/negative similar net charges as a result of the induced surface dipole. 2D LCPD maps the spatial confinement of the induced charges to be localized about 1 graphene unit cell around the dopant sites. Our findings unambiguously show nitrogen and boron dopants tailor graphene chemical reactivity by localized net charges with opposite polarity. Our investigation further insight on to non-covalent interactions of doped graphene with CO. We envision to extend our results to investigate the interaction to other small molecules such CO_2, H_2O or N_2O which is of relevance for the future development of graphene-based molecular sensors

5 Experimental methods

Boron doped Graphene on SiC(0001) was grown as described in Section.2.2.1. N atom implantation was achieved by sputtering the graphene sample with N atoms accelerated at 120 eV and subsequent annealing up to T $\approx$ 1070 K as seen in Section.2.2. STM/AFM measurements were carried out in a UHV chamber equipped with a low-temperature STM/AFM with a qPlus tuning fork sensor operated at 5 K (Createc GmbH). During the AFM measurements, a Pt/Ir tip mounted onto the sensor (frequency $\approx$ 30 kHz; stiffness $\approx$ 1800 N/m) was oscillated with a constant amplitude of 50 pm. To obtain high-resolution AFM/STM images, prior to the experiment, the tip was functionalized with a CO molecule gathered from an Au(111) surface.

For the LCPD mapping in the XZ plane on both dopants, 1250 KPFM measurements were performed with a bias range of [-500 mV, 300 mV] in a grid of size of 3 nm x 1 nm with a step of $x_{step} = 125$ pm, $x_{step} = 20$ pm. The acquisition time for each parabola was 30 s. The mapping was generated by fitting each parabola by the formula$\Delta f(V) = a \cdot (V_{Bias} - LCPD)^2 + c$ with a Python script and assigning the fitted value of the LCPD for every (x,z) position to a 25 x 50 grid of pixels. STM/AFM images were analyzed using WSxM software [72].

References

[1] K. S. Novoselov et al. "Two-dimensional gas of massless Dirac fermions in graphene". In: *Nature* 438.7065 (Nov. 2005), pp. 197–200. DOI: 10.1038/nature04233. URL: https://doi.org/10.1038/nature04233.

[2] A. K. Geim and K. S. Novoselov. "The rise of graphene". In: *Nature Materials* 6.3 (Mar. 2007), pp. 183–191. DOI: 10.1038/nmat1849. URL: https://doi.org/10.1038/nmat1849.

[3] Tapas Kuila et al. "Chemical functionalization of graphene and its applications". In: *Progress in Materials Science* 57.7 (Sept. 2012), pp. 1061–1105. DOI: 10.1016/j.pmatsci.2012.03.002. URL: https://doi.org/10.1016/j.pmatsci.2012.03.002.

[4] Jun Liu et al. "Graphene-based materials for energy applications". In: *MRS Bulletin* 37.12 (Nov. 2012), pp. 1265–1272. DOI: 10.1557/mrs.2012.179. URL: https://doi.org/10.1557/mrs.2012.179.

[5] Seba S. Varghese et al. "Recent advances in graphene based gas sensors". In: *Sensors and Actuators B: Chemical* 218 (Oct. 2015), pp. 160–

183. DOI: 10.1016/j.snb.2015.04.062. URL: https://doi.org/10.1016/j.snb.2015.04.062.

[6] Dimitrios Bitounis et al. "Prospects and Challenges of Graphene in Biomedical Applications". In: *Advanced Materials* 25.16 (Mar. 2013), pp. 2258–2268. DOI: 10.1002/adma.201203700. URL: https://doi.org/10.1002/adma.201203700.

[7] Xiao Huang et al. "Graphene-Based Materials: Synthesis, Characterization, Properties, and Applications". In: *Small* 7.14 (June 2011), pp. 1876–1902. DOI: 10.1002/smll.201002009. URL: https://doi.org/10.1002/smll.201002009.

[8] A. H. Castro Neto et al. "The electronic properties of graphene". In: *Reviews of Modern Physics* 81.1 (Jan. 2009), pp. 109–162. DOI: 10.1103/revmodphys.81.109. URL: https://doi.org/10.1103/revmodphys.81.109.

[9] K. S. Novoselov. "Electric Field Effect in Atomically Thin Carbon Films". In: *Science* 306.5696 (Oct. 2004), pp. 666–669. DOI: 10.1126/science.1102896. URL: https://doi.org/10.1126/science.1102896.

[10] Daniel R. Cooper et al. “Experimental Review of Graphene”. In: *ISRN Condensed Matter Physics* 2012 (2012), pp. 1–56. DOI: 10.5402/2012/501686. URL: https://doi.org/10.5402/2012/501686.

[11] Alexander S. Mayorov et al. “Micrometer-Scale Ballistic Transport in Encapsulated Graphene at Room Temperature”. In: *Nano Letters* 11.6 (June 2011), pp. 2396–2399. DOI: 10.1021/nl200758b. URL: https://doi.org/10.1021/nl200758b.

[12] Wi Hyoung Lee et al. “Surface-Directed Molecular Assembly of Pentacene on Monolayer Graphene for High-Performance Organic Transistors”. In: *Journal of the American Chemical Society* 133.12 (Mar. 2011), pp. 4447–4454. DOI: 10.1021/ja1097463. URL: https://doi.org/10.1021/ja1097463.

[13] Alexander A. Balandin. “Thermal properties of graphene and nanostructured carbon materials”. In: *Nature Materials* 10.8 (July 2011), pp. 569–581. DOI: 10.1038/nmat3064. URL: https://doi.org/10.1038/nmat3064.

[14] Kian Ping Loh et al. “The chemistry of graphene”. In: *Journal of Materials Chemistry* 20.12 (2010), p. 2277. DOI: 10.1039/b920539j. URL: https://doi.org/10.1039/b920539j.

[15] Ado Jorio *et al. Raman Spectroscopy in Graphene Related Systems. The Science of Microfabrication.* Wiley, 2011.

[16] Theanne Schiros et al. "Connecting Dopant Bond Type with Electronic Structure in N-Doped Graphene". In: *Nano Letters* 12.8 (July 2012), pp. 4025–4031. DOI: 10.1021/nl301409h. URL: https://doi.org/10.1021/nl301409h.

[17] Haibo Wang, Thandavarayan Maiyalagan, and Xin Wang. "Review on Recent Progress in Nitrogen-Doped Graphene: Synthesis, Characterization, and Its Potential Applications". In: *ACS Catalysis* 2.5 (Apr. 2012), pp. 781–794. DOI: 10.1021/cs200652y. URL: https://doi.org/10.1021/cs200652y.

[18] Liuyan Zhao et al. "Local Atomic and Electronic Structure of Boron Chemical Doping in Monolayer Graphene". In: *Nano Letters* 13.10 (Sept. 2013), pp. 4659–4665. DOI: 10.1021/nl401781d. URL: https://doi.org/10.1021/nl401781d.

[19] Mykola Telychko et al. "Electronic and Chemical Properties of Donor, Acceptor Centers in Graphene". In: *ACS Nano* 9.9 (Aug. 2015), pp. 9180–9187. DOI: 10.1021/acsnano.5b03690. URL: https://doi.org/10.1021/acsnano.5b03690.

[20] J. Sforzini et al. “Transformation of metallic boron into substitutional dopants in graphene on6H-SiC(0001)”. In: *Physical Review B* 93.4 (Jan. 2016). DOI: 10.1103/physrevb.93.041302. URL: https://doi.org/10.1103/physrevb.93.041302.

[21] Sebastian Wickenburg et al. “Tuning charge and correlation effects for a single molecule on a graphene device”. In: *Nature Communications* 7.1 (Nov. 2016). DOI: 10.1038/ncomms13553. URL: https://doi.org/10.1038/ncomms13553.

[22] Martin Pumera. “Graphene-based nanomaterials and their electrochemistry”. In: *Chemical Society Reviews* 39.11 (2010), p. 4146. DOI: 10.1039/c002690p. URL: https://doi.org/10.1039/c002690p.

[23] Da Chen, Longhua Tang, and Jinghong Li. “Graphene-based materials in electrochemistry”. In: *Chemical Society Reviews* 39.8 (2010), p. 3157. DOI: 10.1039/b923596e. URL: https://doi.org/10.1039/b923596e.

[24] Yuxin Liu, Xiaochen Dong, and Peng Chen. “Biological and chemical sensors based on graphene materials”. In: *Chem. Soc. Rev.* 41.6 (2012), pp. 2283–2307. DOI: 10.1039/c1cs15270j. URL: https://doi.org/10.1039/c1cs15270j.

[25] F. Schedin et al. “Detection of individual gas molecules adsorbed on graphene”. In: *Nature Materials* 6.9 (July 2007), pp. 652–655. DOI: 10.1038/nmat1967. URL: https://doi.org/10.1038/nmat1967.

[26] Ruitao Lv et al. “Nitrogen-doped graphene: beyond single substitution and enhanced molecular sensing”. In: *Scientific Reports* 2.1 (Aug. 2012). DOI: 10.1038/srep00586. URL: https://doi.org/10.1038/srep00586.

[27] Roberto Otero et al. “Molecular Self-Assembly at Solid Surfaces”. In: *Advanced Materials* 23.44 (Sept. 2011), pp. 5148–5176. DOI: 10.1002/adma.201102022. URL: https://doi.org/10.1002/adma.201102022.

[28] Qing Hua Wang and Mark C. Hersam. “Room-temperature molecular-resolution characterization of self-assembled organic monolayers on epitaxial graphene”. In: *Nature Chemistry* 1.3 (May 2009), pp. 206–211. DOI: 10.1038/nchem.212. URL: https://doi.org/10.1038/nchem.212.

[29] Guo Hong et al. “Recent progress in organic molecule/graphene interfaces”. In: *Nano Today* 8.4 (Aug. 2013), pp. 388–402. DOI: 10.1016/j.nantod.2013.07.003. URL: https://doi.org/10.1016/j.nantod.2013.07.003.

[30] J. M. MacLeod and F. Rosei. "Molecular Self-Assembly on Graphene". In: *Small* 10.6 (Oct. 2013), pp. 1038–1049. DOI: 10.1002/smll.201301982. URL: https://doi.org/10.1002/smll.201301982.

[31] Avijit Kumar, Kaustuv Banerjee, and Peter Liljeroth. "Molecular assembly on two-dimensional materials". In: *Nanotechnology* 28.8 (Jan. 2017), p. 082001. DOI: 10.1088/1361-6528/aa564f. URL: https://doi.org/10.1088/1361-6528/aa564f.

[32] Ana Martıén-Recio et al. "Combining nitrogen substitutional defects and oxygen intercalation to control the graphene corrugation and doping level". In: *Carbon* 130 (Apr. 2018), pp. 362–368. DOI: 10.1016/j.carbon.2017.12.117. URL: https://doi.org/10.1016/j.carbon.2017.12.117.

[33] P. Merino et al. "Ortho and Para Hydrogen Dimers on G/SiC(0001): Combined STM and DFT Study". In: *Langmuir* 31.1 (Dec. 2014), pp. 233–239. DOI: 10.1021/la504021x. URL: https://doi.org/10.1021/la504021x.

[34] W. Norimatsu and M. Kusunoki. "Formation process of graphene on SiC (0001)". In: *Physica E: Low-dimensional Systems and Nanostructures* 42.4 (Feb. 2010), pp. 691–694. DOI: 10.1016/j.physe.2009.11.151. URL: https://doi.org/10.1016/j.physe.2009.11.151.

[35] G. Binnig et al. “Surface Studies by Scanning Tunneling Microscopy”. In: *Physical Review Letters* 49.1 (July 1982), pp. 57–61. DOI: 10.1103/physrevlett.49.57. URL: https://doi.org/10.1103/physrevlett.49.57.

[36] G. Binnig, C. F. Quate, and Ch. Gerber. “Atomic Force Microscope”. In: *Physical Review Letters* 56.9 (Mar. 1986), pp. 930–933. DOI: 10.1103/physrevlett.56.930. URL: https://doi.org/10.1103/physrevlett.56.930.

[37] Franz J. Giessibl. “The qPlus sensor, a powerful core for the atomic force microscope”. In: *Review of Scientific Instruments* 90.1 (Jan. 2019), p. 011101. DOI: 10.1063/1.5052264. URL: https://doi.org/10.1063/1.5052264.

[38] F. J. Giessibl. “A direct method to calculate tip–sample forces from frequency shifts in frequency-modulation atomic force microscopy”. In: *Applied Physics Letters* 78.1 (Jan. 2001), pp. 123–125. DOI: 10.1063/1.1335546. URL: https://doi.org/10.1063/1.1335546.

[39] John E Sader et al. “Quantitative force measurements using frequency modulation atomic force microscopy?theoretical foundations”. In: *Nanotechnology* 16.3 (Jan. 2005), S94–S101. DOI: 10.1088/0957-4484/16/3/018. URL: https://doi.org/10.1088/0957-4484/16/3/018.

[40] ScientiaOmicron. *QPlus sensor mounted on an exchangeable tip carrier.* [Online; accessed April 20, 2019]. 2019. URL: https://www.scientaomicron.com/en/products/large-sample-spm/variants.

[41] L. Gross et al. "Measuring the Charge State of an Adatom with Noncontact Atomic Force Microscopy". In: *Science* 324.5933 (June 2009), pp. 1428–1431. DOI: 10.1126/science.1172273. URL: https://doi.org/10.1126/science.1172273.

[42] P. Mallet et al. "Electron states of mono- and bilayer graphene on SiC probed by scanning-tunneling microscopy". In: *Physical Review B* 76.4 (July 2007). DOI: 10.1103/physrevb.76.041403. URL: https://doi.org/10.1103/physrevb.76.041403.

[43] Mykola Telychko et al. "Achieving High-Quality Single-Atom Nitrogen Doping of Graphene/SiC(0001) by Ion Implantation and Subsequent Thermal Stabilization". In: *ACS Nano* 8.7 (June 2014), pp. 7318–7324. DOI: 10.1021/nn502438k. URL: https://doi.org/10.1021/nn502438k.

[44] L. Zhao et al. "Visualizing Individual Nitrogen Dopants in Monolayer Graphene". In: *Science* 333.6045 (Aug. 2011), pp. 999–1003. DOI: 10.1126/science.1208759. URL: https://doi.org/10.1126/science.1208759.

[45] G. M. Rutter et al. "Scattering and Interference in Epitaxial Graphene". In: *Science* 317.5835 (July 2007), pp. 219–222. DOI: 10.1126/science.1142882. URL: https://doi.org/10.1126/science.1142882.

[46] I. Brihuega et al. "Quasiparticle Chirality in Epitaxial Graphene Probed at the Nanometer Scale". In: *Physical Review Letters* 101.20 (Nov. 2008). DOI: 10.1103/physrevlett.101.206802. URL: https://doi.org/10.1103/physrevlett.101.206802.

[47] R. J. Hamers, R. M. Tromp, and J. E. Demuth. "Surface Electronic Structure of Si (111)-(7×7) Resolved in Real Space". In: *Physical Review Letters* 56.18 (May 1986), pp. 1972–1975. DOI: 10.1103/physrevlett.56.1972. URL: https://doi.org/10.1103/physrevlett.56.1972.

[48] Alex W. Robertson et al. "Spatial control of defect creation in graphene at the nanoscale". In: *Nature Communications* 3.1 (Jan. 2012). DOI: 10.1038/ncomms2141. URL: https://doi.org/10.1038/ncomms2141.

[49] L. Gross et al. "The Chemical Structure of a Molecule Resolved by Atomic Force Microscopy". In: *Science* 325.5944 (Aug. 2009), pp. 1110–1114. DOI: 10.1126/science.1176210. URL: https://doi.org/10.1126/science.1176210.

[50] Shigeki Kawai et al. “Van der Waals interactions and the limits of isolated atom models at interfaces”. In: *Nature Communications* 7.1 (May 2016). DOI: 10.1038/ncomms11559. URL: https://doi.org/10.1038/ncomms11559.

[51] Leo Gross et al. “Organic structure determination using atomic-resolution scanning probe microscopy”. In: *Nature Chemistry* 2.10 (Aug. 2010), pp. 821–825. DOI: 10.1038/nchem.765. URL: https://doi.org/10.1038/nchem.765.

[52] D. G. de Oteyza et al. “Direct Imaging of Covalent Bond Structure in Single-Molecule Chemical Reactions”. In: *Science* 340.6139 (May 2013), pp. 1434–1437. DOI: 10.1126/science.1238187. URL: https://doi.org/10.1126/science.1238187.

[53] Pavel Jelínek. “High resolution SPM imaging of organic molecules with functionalized tips”. In: *Journal of Physics: Condensed Matter* 29.34 (July 2017), p. 343002. DOI: 10.1088/1361-648x/aa76c7. URL: https://doi.org/10.1088/1361-648x/aa76c7.

[54] Bruno de la Torre et al. “Non-covalent control of spin-state in metal-organic complex by positioning on N-doped graphene”. In: *Nature Communications* 9.1 (July 2018). DOI: 10.1038/s41467-018-05163-y. URL: https://doi.org/10.1038/s41467-018-05163-y.

[55] L. Gross et al. “Bond-Order Discrimination by Atomic Force Microscopy”. In: *Science* 337.6100 (Sept. 2012), pp. 1326–1329. DOI: 10.1126/science.1225621. URL: https://doi.org/10.1126/science.1225621.

[56] Shigeki Kawai et al. “Multiple heteroatom substitution to graphene nanoribbon”. In: *Science Advances* 4.4 (Apr. 2018), eaar7181. DOI: 10.1126/sciadv.aar7181. URL: https://doi.org/10.1126/sciadv.aar7181.

[57] Prokop Hapala et al. “Mechanism of high-resolution STM/AFM imaging with functionalized tips”. In: *Physical Review B* 90.8 (Aug. 2014). DOI: 10.1103/physrevb.90.085421. URL: https://doi.org/10.1103/physrevb.90.085421.

[58] Prokop Hapala et al. “Mapping the electrostatic force field of single molecules from high-resolution scanning probe images”. In: *Nature Communications* 7.1 (May 2016). DOI: 10.1038/ncomms11560. URL: https://doi.org/10.1038/ncomms11560.

[59] P. E. Blöchl. “Projector augmented-wave method”. In: *Physical Review B* 50.24 (Dec. 1994), pp. 17953–17979. DOI: 10.1103/physrevb.50.17953. URL: https://doi.org/10.1103/physrevb.50.17953.

[60] G. Kresse and D. Joubert. "From ultrasoft pseudopotentials to the projector augmented-wave method". In: *Physical Review B* 59.3 (Jan. 1999), pp. 1758–1775. DOI: 10.1103/physrevb.59.1758. URL: https://doi.org/10.1103/physrevb.59.1758.

[61] Jiřıé Klimeš, David R. Bowler, and Angelos Michaelides. "Van der Waals density functionals applied to solids". In: *Physical Review B* 83.19 (May 2011). DOI: 10.1103/physrevb.83.195131. URL: https://doi.org/10.1103/physrevb.83.195131.

[62] Petr Lazar et al. "Adsorption of Small Organic Molecules on Graphene". In: *Journal of the American Chemical Society* 135.16 (Apr. 2013), pp. 6372–6377. DOI: 10.1021/ja403162r. URL: https://doi.org/10.1021/ja403162r.

[63] Fabian Mohn et al. "Imaging the charge distribution within a single molecule". In: *Nature Nanotechnology* 7.4 (Feb. 2012), pp. 227–231. DOI: 10.1038/nnano.2012.20. URL: https://doi.org/10.1038/nnano.2012.20.

[64] Franck Bocquet, Laurent Nony, and Christian Loppacher. "Polarization effects in noncontact atomic force microscopy: A key to model the tip-sample interaction above charged adatoms". In: *Physical Review B* 83.3

(Jan. 2011). DOI: 10.1103/physrevb.83.035411. URL: https://doi.org/10.1103/physrevb.83.035411.

[65] Fredrik Sydow Hage et al. "Local Plasmon Engineering in Doped Graphene". In: *ACS Nano* 12.2 (Feb. 2018), pp. 1837–1848. DOI: 10.1021/acsnano.7b08650. URL: https://doi.org/10.1021/acsnano.7b08650.

[66] Paolo Marconcini et al. "Atomistic Boron-Doped Graphene Field-Effect Transistors: A Route toward Unipolar Characteristics". In: *ACS Nano* 6.9 (Aug. 2012), pp. 7942–7947. DOI: 10.1021/nn3024046. URL: https://doi.org/10.1021/nn3024046.

[67] Aurélien Lherbier, Andrés Rafael Botello-Méndez, and Jean-Christophe Charlier. "Electronic and Transport Properties of Unbalanced Sublattice N-Doping in Graphene". In: *Nano Letters* 13.4 (Mar. 2013), pp. 1446–1450. DOI: 10.1021/nl304351z. URL: https://doi.org/10.1021/nl304351z.

[68] Lingmei Kong et al. "Molecular adsorption on graphene". In: *Journal of Physics: Condensed Matter* 26.44 (Oct. 2014), p. 443001. DOI: 10.1088/0953-8984/26/44/443001. URL: https://doi.org/10.1088/0953-8984/26/44/443001.

[69] Jongweon Cho et al. “Structural and Electronic Decoupling of C60 from Epitaxial Graphene on SiC”. In: *Nano Letters* 12.6 (May 2012), pp. 3018–3024. DOI: 10.1021/nl3008049. URL: https://doi.org/10.1021/nl3008049.

[70] Vasilios Georgakilas et al. “Functionalization of Graphene: Covalent and Non-Covalent Approaches, Derivatives and Applications”. In: *Chemical Reviews* 112.11 (Sept. 2012), pp. 6156–6214. DOI: 10.1021/cr3000412. URL: https://doi.org/10.1021/cr3000412.

[71] Van Dong Pham et al. “Selective control of molecule charge state on graphene using tip-induced electric field and nitrogen doping”. In: *npj 2D Materials and Applications* 3.1 (Jan. 2019). DOI: 10.1038/s41699-019-0087-5. URL: https://doi.org/10.1038/s41699-019-0087-5.

[72] I. Horcas et al. “WSXM: A software for scanning probe microscopy and a tool for nanotechnology”. In: *Review of Scientific Instruments* 78.1 (Jan. 2007), p. 013705. DOI: 10.1063/1.2432410. URL: https://doi.org/10.1063/1.2432410.